



## Abstract

The atmospheric chemistry general circulation model ECHAM5/MESSy is used to simulate polar surface air temperature effects of geomagnetic activity variations. A transient model simulation was performed for the years 1960–2004 and is shown to develop polar surface air temperature patterns that depend on geomagnetic activity strength, similar to previous studies. In order to eliminate influencing factors such as sea surface temperatures (SST) or UV variations, two nine-year long simulations were carried out, with strong and weak geomagnetic activity, respectively, while all other boundary conditions were held to year 2000 levels. Statistically significant temperature effects that were observed in previous reanalysis and model results are also obtained from this set of simulations, suggesting that such patterns are indeed related to geomagnetic activity. In the model, strong geomagnetic activity and the associated NO<sub>x</sub> enhancements lead to polar stratospheric ozone loss. Compared with the simulation with weak geomagnetic activity, the ozone loss causes a decrease in ozone radiative cooling and thus a temperature increase in the polar winter mesosphere. Similar to previous studies, a cooling is found below the stratopause, which other authors have attributed to a decrease in the mean meridional circulation. In the polar stratosphere this leads to a more stable vortex. A strong (weak) Northern Hemisphere vortex is known to be associated with a positive (negative) Northern Annular Mode (NAM) index; our simulations exhibit a positive NAM index for strong geomagnetic activity, and a negative NAM for weak geomagnetic activity. Such NAM anomalies have been shown to propagate to the surface, and this is also seen in the model simulations. NAM anomalies are known to lead to specific surface temperature anomalies: a positive NAM is associated with warmer than average northern Eurasia and colder than average eastern North Atlantic. This is also the case in our simulation. Our simulations suggest a link between geomagnetic activity, ozone loss, stratospheric cooling, the NAM, and surface temperature variability.

### High altitude NO<sub>x</sub> modulation of the NAM index

A. J. G. Baumgaertner  
et al.

Title Page

Abstract

Introduction

Conclusions

References

Tables

Figures

⏪

⏩

◀

▶

Back

Close

Full Screen / Esc

Printer-friendly Version

Interactive Discussion



## 1 Introduction

Solar variability manifests itself in several different ways. Amongst them is the variability of the solar wind, a stream of mainly electrons and protons that are able to escape the sun's upper atmosphere. When the solar wind interacts with the Earth's magnetosphere, the magnetosphere can experience a loss of charged particles through precipitation into the Earth's upper and middle atmosphere at high geomagnetic latitudes (Clilverd et al., 2006). There, the energetic particle precipitation leads to  $\text{NO}_x$  (=  $\text{NO} + \text{NO}_2$ ) production (EPP- $\text{NO}_x$ ) by dissociation of nitrogen. It has been found that the amount of  $\text{NO}_x$  produced corresponds to the level of geomagnetic activity (Siskind et al., 2000; Hood and Soukharev, 2006; Randall et al., 2007), ultimately linking it to solar variability. During polar winter, EPP- $\text{NO}_x$  can live long enough to be transported into the stratosphere and engage in catalytic ozone destruction. Several studies have shown the importance of this process in the polar upper stratosphere (Randall et al., 2005; Funke et al., 2005; Baumgaertner et al., 2009; Seppälä et al., 2007b,a).

Generally, however, in sun-earth connection studies EPP- $\text{NO}_x$  has not been regarded as important as variations in ultraviolet irradiance, which can exceed 50% at some wavelengths. Such variations have been shown to lead to stratospheric ozone changes and induce temperature variations over the 11 year solar cycle (e.g. Austin et al., 2008) as well as the 27 day solar rotation period (e.g. Gruzdev et al., 2009). The type and magnitude of any response to such solar variability at the surface is still not understood (Meehl et al., 2009; IPCC, 2007).

A number of publications have addressed the possible connections of changes in polar climate and solar or geomagnetic activity, but they generally do not consider EPP- $\text{NO}_x$ . For example, Boberg and Lundstedt (2002) have suggested a link between the electric field strength of the solar wind and the phase of the North Atlantic Oscillation (NAO). Recent studies have raised the question whether there could be effects at the surface level due to EPP- $\text{NO}_x$ . Thejll et al. (2003) found a correlation between the Ap index (which is derived from magnetic field component measurements at 13 subauroral

### High altitude $\text{NO}_x$ modulation of the NAM index

A. J. G. Baumgaertner et al.

Title Page

Abstract

Introduction

Conclusions

References

Tables

Figures



Back

Close

Full Screen / Esc

Printer-friendly Version

Interactive Discussion

---

**High altitude NO<sub>x</sub>  
modulation of the  
NAM index**A. J. G. Baumgaertner  
et al.

---

[Title Page](#)[Abstract](#)[Introduction](#)[Conclusions](#)[References](#)[Tables](#)[Figures](#)[⏪](#)[⏩](#)[◀](#)[▶](#)[Back](#)[Close](#)[Full Screen / Esc](#)[Printer-friendly Version](#)[Interactive Discussion](#)

geomagnetic observatories (Mayaud, 1980)) and the NAO since about 1970. Rozanov et al. (2005) first suggested that polar surface temperatures might be affected by EPP-NO<sub>x</sub>. Seppälä et al. (2009) were the first to show that in the ECMWF ERA-40 reanalysis data set (Uppala et al., 2005) wintertime polar surface temperatures have different patterns during years of high and low geomagnetic activity. Lu et al. (2008) investigated EPP-NO<sub>x</sub> influences on springtime polar stratospheric dynamics also using the ERA-40 data set. Their results suggested that changes observed in stratospheric winds and temperatures were unlikely to be caused in situ in the stratosphere by EPP-NO<sub>x</sub> but were rather due to an indirect dynamical link, e.g. wave activity.

In this paper we present an analysis of surface air temperatures (SAT) and their relationship to EPP-NO<sub>x</sub> using a transient simulation with the ECHAM5/MESSy Atmospheric Chemistry (EMAC) model, which is described in Sect. 2.1. The results, covering a similar time period as that in the ERA-40 study by Seppälä et al. (2009), are presented in Sect. 3.1. In order to eliminate aliasing of other sources of variability we further compare two EMAC simulations, where boundary conditions are repeated and the EPP-NO<sub>x</sub> is switched on/off (Sect. 3.2). The physical link between EPP-NO<sub>x</sub> and SAT is discussed in Sect. 3.3. Particular emphasis is given here to the analysis of the Northern Hemisphere (NH) because of the robustness of the results. Southern Hemisphere (SH) results are more difficult to interpret and are only briefly discussed here, warranting further studies.

## 2 Model description

### 2.1 ECHAM5/MESSy

The ECHAM5/MESSy Atmospheric Chemistry (EMAC) model is a numerical chemistry and climate simulation system that includes submodels describing tropospheric and middle atmosphere processes and their interaction with oceans, land and human influences (Jöckel et al., 2006, 2010). It uses the Modular Earth Submodel System

(MESSy) to link multi-institutional computer codes. The core atmospheric model is the 5th generation European Centre Hamburg general circulation model (ECHAM5, Roeckner et al., 2006). The model has been shown to consistently simulate key atmospheric tracers such as ozone (Jöckel et al., 2006), water vapour (Lelieveld et al., 2007), and lower and middle stratospheric  $\text{NO}_y = \text{HNO}_3 + \text{NO} + \text{NO}_2 + 2\text{N}_2\text{O}_5 + \text{HNO}_4 + \text{ClONO}_2$  (Brühl et al., 2007). For the present study we applied EMAC (ECHAM5 version 5.3.01, MESSy version 1.6 for the transient study, see Sect. 3.1, and ECHAM5 version 5.3.02, MESSy version 1.8+ for the sensitivity study, see Sect. 3.2) in the T42L90MA-resolution, i.e., with a spherical truncation of T42 (corresponding to a quadratic Gaussian grid of approx. 2.8 by 2.8 degrees in latitude and longitude) with 90 vertical hybrid pressure levels up to 0.01 hPa. This part of the setup matches the model evaluation study by Jöckel et al. (2006). Enabled submodels are also the same as in Jöckel et al. (2006) apart from the additional submodel SPACENOX (details see below), a more detailed treatment of the solar variation in the photolysis submodel JVAL, and the sub-submodel FUBRad (Nissen et al., 2007), a high-resolution short-wave heating rate parameterization. The chosen chemistry scheme for the configuration of the submodel MECCA (Sander et al., 2005) is simpler compared with the configuration in Jöckel et al. (2006). For example, the NMHC (non-methane hydrocarbon) chemistry is not treated at the same level of detail. The complete mechanism is documented in the electronic supplement.

The parameterization for  $\text{NO}_x$  production by particle precipitation at the model top (submodel SPACENOX) is described and evaluated by Baumgaertner et al. (2009). It is based on the Ap index and was designed such that stratospheric  $\text{NO}_x$  amounts resemble those observed by Randall et al. (2005) and Funke et al. (2005). The public review process of Baumgaertner et al. (2009) identified that the parameterization could be improved by lagging  $\text{NO}_x$  production in the model by several weeks with respect to the Ap index in order to account for the time the EPP- $\text{NO}_x$  needs to be transported into the model domain. This has been implemented and a lag of one month was used for the present study.

## High altitude $\text{NO}_x$ modulation of the NAM index

A. J. G. Baumgaertner et al.

Title Page

Abstract

Introduction

Conclusions

References

Tables

Figures

◀

▶

◀

▶

Back

Close

Full Screen / Esc

Printer-friendly Version

Interactive Discussion



### 3 Results and discussion

#### 3.1 Transient simulation

A comprehensive simulation covering the period 1960 to 2004 was carried out to study solar variability effects, including photolysis and heating rate variations using the high-resolution short-wave code FUBRad (Nissen et al., 2007), as well as particle precipitation effects (Baumgaertner et al., 2010, 2009). The description of the simulation and results concerning middle atmosphere effects resulting from solar activity variations will be presented elsewhere. Here, we present surface air temperature results from this simulation, which hereafter is denoted as S-TRANSIENT. The analysis is performed analogously to Seppälä et al. (2009) in that the dataset was separated according to the yearly average wintertime Ap index, used as proxy for the overall geomagnetic activity level. The analysis is done separately for the Northern and Southern Hemisphere. The division to high and low geomagnetic activity years according to the Ap index is summarised in Table 1. The mean Ap value of 13.5 was used as a threshold for the high-low separation.

The NH temperature difference  $\Delta T = \text{High Ap} - \text{Low Ap}$  for the winter season DJF (December-January-February) is presented in Fig. 1 for the simulation results (left) and the reanalysis (right), taken from Seppälä et al. (2009). There are some remarkable similarities between the temperature patterns found in the simulation and the ERA-40 reanalysis (Seppälä et al., 2009, see their Figs. 2 and 3). Both the reanalysis data and the model show a negative anomaly of about 2 K over the North Atlantic, and a positive anomaly over the Arctic Sea, especially pronounced east of Greenland. The strongest warm anomaly is situated over Siberia in the reanalysis data, the model, however, shows this warm anomaly approximately centred around Svalbard. It should be noted that a perfect pattern match between the model and the reanalysis is not expected because the dynamics of the model were not relaxed to the observed meteorology. Hence, the synoptic situation in the model is different to the situation in the reanalysis at any given time. The model was however driven with observed sea

## High altitude NO<sub>x</sub> modulation of the NAM index

A. J. G. Baumgaertner et al.

Title Page

Abstract

Introduction

Conclusions

References

Tables

Figures



Back

Close

Full Screen / Esc

Printer-friendly Version

Interactive Discussion



---

**High altitude NO<sub>x</sub>  
modulation of the  
NAM index**A. J. G. Baumgaertner  
et al.

---

[Title Page](#)[Abstract](#)[Introduction](#)[Conclusions](#)[References](#)[Tables](#)[Figures](#)[⏪](#)[⏩](#)[◀](#)[▶](#)[Back](#)[Close](#)[Full Screen / Esc](#)[Printer-friendly Version](#)[Interactive Discussion](#)

surface temperatures (SST) and sea ice masks (HadISST1, see Rayner et al., 2003), which are expected to influence the SAT. Therefore, SST interannual variability can lead to aliasing effects in the SAT patterns described above. The same years as used for the surface temperature calculation were used for Fig. 2 which shows the difference between the SSTs in years of high and low geomagnetic activity. The differences are generally smaller than 1 K and thus unlikely to alias the surface temperature result presented above. However, sensitivity simulations using boundary conditions from a single year are presented in the next section, completely eliminating the possibility of aliasing of SSTs and other influencing factors such as UV variability. Seppälä et al. (2009) considered the influence of sudden stratospheric warmings (SSW) on their results, which lead them to exclude years with SSWs from the analysis (see their Fig. 3). This is not possible for the model results because SSWs did not occur in the same years as in the reanalysis, and therefore different years would have to be excluded.

Figure 3 depicts the SH temperature differences for the months JJA (June–July–August) for which Seppälä et al. (2009) found the largest anomalies in the SH. Note that only years from 1979 onward were used here to be consistent with the study by Seppälä et al. (2009). The model and reanalysis (Fig. 6 of Seppälä et al., 2009) again show similar temperature patterns. The Antarctic peninsula is warmer by approximately 2 K, and the area east of the Ross Sea is colder by up to 4 K. However, the model also shows a distinct cold anomaly in East Antarctica, which is absent in the reanalysis dataset. This might be due to the sparse measurement density there, but could also be a result of the small number of years used for analysing the SH. In the following, we will mainly focus on the NH temperature pattern due to the larger number of years available for that region thus improving the statistics. Further problems associated with the SH pattern will be discussed in Sect. 3.2.

In order to quantify the agreement between the simulated and observed SAT patterns, and to judge its statistical significance, we performed the following analysis: we calculated the Pearson correlation coefficient between the model SAT and the ERA-40 SAT pattern as shown in Fig. 1 by interpolation of the ERA-40 data onto the model grid

---

## High altitude NO<sub>x</sub> modulation of the NAM index

A. J. G. Baumgaertner  
et al.

---

[Title Page](#)[Abstract](#)[Introduction](#)[Conclusions](#)[References](#)[Tables](#)[Figures](#)[◀](#)[▶](#)[◀](#)[▶](#)[Back](#)[Close](#)[Full Screen / Esc](#)[Printer-friendly Version](#)[Interactive Discussion](#)

and interpreting the two gridded datasets as vectors. The obtained correlation coefficient is 0.35. Note that this analysis cannot account for example for shifts of maxima or minima. To enable a better interpretation of the correlation coefficient, we repeatedly calculated the correlation coefficient between DJF SAT temperatures of random model years (uniformly distributed; same number of years in the “low” and “high” categories as in Table 1) and the ERA-40 data. From 100 different sets the mean correlation coefficient was found to be  $-0.01$ ; ignoring the sign of each correlation coefficient yields a mean of 0.25. In the light of these findings the correlation coefficient of 0.35 warrants further analysis of the phenomenon.

In order to show that in the model the geomagnetic activity related NO<sub>x</sub> changes in the polar stratosphere are not masked by dynamical influence, we calculated the correlation between the mean Ap index (November-December-January average) north of 60° N and the NO<sub>x</sub> mixing ratio at 45 km (December-January-February average) which is shown in Fig. 4. The resulting correlation coefficient is 0.83. A similar result is obtained if only the years listed in Table 1 are used (denoted by red stars; correlation coefficient: 0.82). Thus, NO<sub>x</sub> enhancements produced by strong geomagnetic activity lead to significant enhancements in the upper stratosphere, with only a weak dependence on other factors such as variable dynamical conditions that influence vertical or horizontal transport.

### 3.2 Sensitivity study: cyclic boundary conditions

In order to minimise possible aliasing effects of boundary conditions other than geomagnetic activity on the SAT, two additional nine-year simulations were carried out, one with high geomagnetic activity, and one with low geomagnetic activity. They are both based on the setup of the transient simulation described above, except that boundary conditions were taken from the year 2000 and repeated for every year of the simulation. These boundary conditions include:

1. sea surface temperatures and sea ice masks,
2. chemical tracers with a long lifetime, which are “nudged” towards observed values

**High altitude NO<sub>x</sub>  
modulation of the  
NAM index**A. J. G. Baumgaertner  
et al.

Title Page

Abstract

Introduction

Conclusions

References

Tables

Figures

◀

▶

◀

▶

Back

Close

Full Screen / Esc

Printer-friendly Version

Interactive Discussion



at the surface: greenhouse gases (CO<sub>2</sub>, N<sub>2</sub>O, CH<sub>4</sub>), chlorofluorocarbons and halons (CFCl<sub>3</sub>, CF<sub>2</sub>Cl<sub>2</sub>, CH<sub>3</sub>CCl<sub>3</sub>, CCl<sub>4</sub>, CH<sub>3</sub>Cl, CH<sub>3</sub>Br, CF<sub>2</sub>ClBr, CF<sub>3</sub>Br),

- emissions of short-lived tracers: NO, CO, C<sub>2</sub>H<sub>4</sub>, C<sub>2</sub>H<sub>6</sub>, C<sub>4</sub>H<sub>10</sub>, CH<sub>3</sub>CHO, CH<sub>3</sub>COCH<sub>3</sub>, CH<sub>3</sub>COOH, CH<sub>3</sub>OH, HCHO, HCOOH, SO<sub>2</sub>, NH<sub>3</sub>, DMS, NO<sub>x</sub> from aircraft,
- solar flux for photolysis and radiative heating, and the
- geomagnetic activity (EPP-NO<sub>x</sub> input).

The high geomagnetic activity EPP-NO<sub>x</sub>, was taken from the year 2003 because this was one of the most active years in the recent past. For the NH winter (DJF), the mean Ap index, after the applied shift of one month to account for downward transport not captured by the model, was 25.2. For the first simulation, hereafter termed S-EPP, the SPACENOX submodel providing the EPP-NO<sub>x</sub> input at the upper boundary, was switched on. For the second simulation the submodel was turned off, effectively corresponding to years of very low geomagnetic activity, where no NO<sub>x</sub> from the EPP source reaches the mesosphere. This simulation is hereafter referred to as S-noEPP.

It should be noted that cyclic boundary conditions will introduce discontinuities from December to January since they are not taken from consecutive years but rather from the same year. However, the seasonal cycle is strong for SSTs as it is for chemical boundary conditions, therefore this issue is not regarded as problematic.

By subtracting the results of the simulation S-noEPP from the simulation S-EPP (i.e. S-EPP – S-noEPP) the influence of EPP-NO<sub>x</sub> can be extracted. Since the model is free-running, there is also inherent variability, which effectively adds noise to the results. Moreover, as has been pointed out by Seppälä et al. (2009), care has to be taken regarding years with SSWs, which are the strongest manifestation of stratospheric interannual variability. Both simulations were run for nine years, giving a total of 18 NH winters. The NO<sub>x</sub> mixing ratios for the simulation S-EPP are shown in Fig. 6 for a single NH winter. Large NO<sub>x</sub> enhancements are evident that propagate downwards during





the mechanism explaining the SAT anomalies we now discuss the sensitivity simulations in more detail.

As shown by Baumgaertner et al. (2009), geomagnetic activity related polar winter  $\text{NO}_x$  enhancements leads to stratospheric ozone loss due to the catalytic destruction of odd oxygen. Therefore, ozone mixing ratios are expected to be significantly different between the simulations S-EPP and S-noEPP. Ozone differences between these two simulations ( $\Delta O_3 = O_3^{\text{S-EPP}} - O_3^{\text{S-noEPP}}$ ) as a function of latitude and altitude for DJF are shown in Fig. 8.

Indeed, stratospheric ozone is reduced by up to  $1 \mu\text{mol mol}^{-1}$  in the middle and upper stratosphere (approximately 20% in the upper stratosphere, 10% at 20 hPa) in the polar area. This leads to a mean total column ozone loss of up to 35 DU. Since ozone is an important radiatively active gas, in general stratospheric ozone concentration changes lead to effects in temperatures. During polar winter, the affected region is mostly dark, so effects caused by the absorption of solar short-wave radiation are expected to be small. However, ozone is also a radiative coolant, an effective greenhouse gas, and it absorbs longwave radiation from the surface. Ozone changes can therefore potentially lead to temperatures changes even during the polar night. Ozone depletion effects on temperature and dynamics have been subject to intensive research in the past (Langematz et al., 2003; Randel and Wu, 1999; Austin et al., 2001; Shine et al., 2003; Christiansen et al., 1997, and others), mainly focusing on CFC induced ozone depletion. In general, such responses have been shown to be dependent on latitude, season, and on the vertical profile of ozone loss. For the analysis here, a relevant study was conducted by Langematz et al. (2003). Using sensitivity simulations with prescribed ozone loss and a control simulation, they found a heating above the stratopause and cooling below for the NH polar winter (see their Fig. 8a). Using additional radiative transfer calculations, which show only a warming throughout the stratosphere (their Fig. 9a), they concluded that the decrease in ozone radiative cooling is responsible for the warming in the simulation with ozone depletion. The cooling below the stratopause was attributed to dynamical heating induced by a decrease of the mean meridional

## High altitude $\text{NO}_x$ modulation of the NAM index

A. J. G. Baumgaertner et al.

Title Page

Abstract

Introduction

Conclusions

References

Tables

Figures

◀

▶

◀

▶

Back

Close

Full Screen / Esc

Printer-friendly Version

Interactive Discussion



circulation. Figure 9 presents the temperature differences between the two sensitivity simulations performed here. The figure shows that polar lower stratospheric temperatures between 200–5 hPa decrease by up to 4 K in the S-EPP simulation, and above 4 hPa polar temperatures increase in the S-EPP simulation, indicating that the two-fold response described by Langematz et al. (2003) is likely to be also responsible for the effects observed in the EMAC simulations.

Polar stratospheric temperature changes during winter are likely to have an effect on the polar vortex. A quantity that is often used to describe the strength of the vortex is the Northern Annular Mode (NAM) index (Baldwin and Dunkerton, 2001), with positive NAM index values indicating a strong polar vortex and negative index values a weaker vortex. We calculated the NAM index for the model results from the geopotential heights using the zonal mean EOF (empirical orthogonal function) method described by Baldwin and Thompson (2009). The change in the polar (60° N–90° N) zonal mean geopotential height anomalies between the two simulations are presented in Fig. 10. The figure shows how a strong negative anomaly which first develops early in the winter season at higher altitudes and descends downwards reaching the mid-stratosphere by February. Using the model geopotential heights, the NAM index was calculated and histograms of the NAM indices between 10 hPa and the tropopause for DJF are shown in Fig. 11. The solid (dashed) black line is the histogram for the simulation S-EPP (S-noEPP). While the tails of the distribution are similar, the probability for NAM indices within the range  $\pm 2$  is different between the two simulations: positive NAM indices are more likely in the S-EPP simulation, thus indicating a stronger Arctic polar vortex in the S-EPP simulation.

From Baldwin and Dunkerton (2001) and others it is known that anomalous weather regimes characterised by NAM index anomalies can propagate down into the troposphere. This is also observed in the simulations presented here, as shown in Fig. 12, where we focus on a single winter from both simulations (top: S-EPP, bottom: S-noEPP). For example, in this case in the S-EPP simulation a positive NAM anomaly develops in the stratosphere in late December, reaching the surface by mid-January.

## High altitude NO<sub>x</sub> modulation of the NAM index

A. J. G. Baumgaertner et al.

[Title Page](#)[Abstract](#)[Introduction](#)[Conclusions](#)[References](#)[Tables](#)[Figures](#)[⏪](#)[⏩](#)[◀](#)[▶](#)[Back](#)[Close](#)[Full Screen / Esc](#)[Printer-friendly Version](#)[Interactive Discussion](#)

This is not observed in the equivalent S-noEPP simulation.

In the troposphere NAM anomalies are related to weather anomalies (Hurrell and Kushnir, 2003) including specific temperature anomalies. The general characteristic of a positive NAM anomaly is a warmer than average Northern Eurasia, a colder than average Eastern North Atlantic, and a warmer than average United States (see e.g. Hurrell and Kushnir, 2003, chapter 1, Fig. 13). This corresponds to the observed temperature patterns found in the SAT difference between S-EPP and S-noEPP (Fig. 7). The NAM phase can also be detected in the surface pressure. The positive phase is characterised by anomalously low pressures at high latitudes and higher than average pressures at mid-latitudes. Figure 13 depicts the DJF surface pressure differences between the simulations S-EPP and S-noEPP. The negative pressure anomalies over Greenland and positive anomalies at mid-latitudes indicate a positive NAM phase as expected, although the low pressure region does not extend over Scandinavia as the NAM often does. Since the NAM related NAO (see e.g. Hurrell and Kushnir, 2003) index is often calculated as the pressure difference between the Azores and Reykjavik, Iceland, the predicted pattern also influences the NAO index.

In the light of this mechanism, a possible reason for the lack of a similarly significant response in the SH could be the fact that the SH polar vortex is already much colder and more stable than in the NH. This potentially makes it less susceptible to perturbations by NO<sub>x</sub> enhancements. However, the SH response is subject to further work.

## 4 Conclusions

Seppälä et al. (2009) used reanalysis data to show that winter surface air temperatures divided up in years of low and high geomagnetic activity show significant temperature anomalies similar to NAM patterns found at high latitudes. Here, we have shown that this effect is also found in a 44-year transient simulation that used the Ap index to parametrise geomagnetic activity and associated NO<sub>x</sub> production in the middle and upper atmosphere through particle precipitation. In order to avoid aliasing from sea

### High altitude NO<sub>x</sub> modulation of the NAM index

A. J. G. Baumgaertner et al.

Title Page

Abstract

Introduction

Conclusions

References

Tables

Figures

⏪

⏩

◀

▶

Back

Close

Full Screen / Esc

Printer-friendly Version

Interactive Discussion



surface temperatures (SST) and other boundary conditions present in the transient simulation, two additional nine-year simulations were performed, where the boundary conditions were repeated on a yearly basis. The only difference between the two simulations was that geomagnetic activity related NO<sub>x</sub> production was switched on in one simulation, thus allowing us to identify purely NO<sub>x</sub> induced effects. Again, similar surface temperature patterns were found. This indicates that these patterns are indeed related to NO<sub>x</sub> production due to geomagnetic activity. The following mechanism was established from the model results: The geomagnetic activity/Energetic Particle Precipitation related NO<sub>x</sub> production leads to ozone depletion in the stratosphere. As a consequence changes in the radiative budget and subsequently of the mean meridional circulation cool the lower stratosphere and strengthens the polar vortex. Associated positive NAM anomalies propagate into the troposphere, where typical positive NAM surface pressure and temperature patterns occur. Therefore, enhanced geomagnetic activity and NO<sub>x</sub> production appear to trigger positive NAM phases at the surface level in the model. Further studies are required to confirm these results and the proposed mechanism as the findings indicate a stronger link of surface climate to space weather than has previously been assumed.

**Supplementary material related to this article is available online at:**

**<http://www.atmos-chem-phys-discuss.net/10/30171/2010/acpd-10-30171-2010-supplement.pdf>.**

*Acknowledgements.* This research was funded by the TIES project within the DFG SPP 1176 CAUSES. Thanks go to all MESSy developers and users for their support. We thank Cora Randall and Dan Marsh, and Robert Hibbins for fruitful discussions. The model simulations were performed on the POWER-6 computer at the RZG and DKRZ. The Ferret program (<http://www.ferret.noaa.gov>) from NOAA's Pacific Marine Environmental Laboratory was used for creating some of the graphics in this paper. The work of AS was funded through the FP7-PEOPLE-IEF Marie Curie project EPPIC/237461.

The service charges for this open access publication have been covered by the Max Planck Society.

30185

ACPD

10, 30171–30203, 2010

## High altitude NO<sub>x</sub> modulation of the NAM index

A. J. G. Baumgaertner  
et al.

Title Page

Abstract

Introduction

Conclusions

References

Tables

Figures

◀

▶

◀

▶

Back

Close

Full Screen / Esc

Printer-friendly Version

Interactive Discussion



## References

- Austin, J., Langematz, U., Dameris, M., Pawson, S., Pitari, G., Shine, K. P., and Stordal, F.: Stratospheric ozone and its links to climate change, pp. 191–222, Office for Off. Publ. of the Eur. Comm., Luxembourg, 2001. 30182
- 5 Austin, J., Tourpali, K., Rozanov, E., Akiyoshi, H., Bekki, S., Bodeker, G., Brühl, C., Butchart, N., Chipperfield, M., Deushi, M., Fomichev, V. I., Giorgetta, M. A., Gray, L., Kodera, K., Lott, F., Manzini, E., Marsh, D., Matthes, K., Nagashima, T., Shibata, K., Stolarski, R. S., Struthers, H., and Tian, W.: Coupled chemistry climate model simulations of the solar cycle in ozone and temperature, *J. Geophys. Res.*, 113, D11306, doi:10.1029/2007JD009391, 2008. 30173
- 10 Baldwin, M. P. and Dunkerton, T. J.: Stratospheric harbingers of anomalous weather regimes, *Science*, 294, 581–584, doi:10.1126/science.1063315, 2001. 30183
- Baldwin, M. P. and Thompson, D. W. J.: A critical comparison of stratosphere-troposphere coupling indices, *Q. J. Roy. Meteorol. Soc.*, 135, 1661–1672, doi:10.1002/qj.479, 2009. 30183
- Baumgaertner, A. J. G., Jöckel, P., and Brühl, C.: Energetic particle precipitation in ECHAM5/MESSy1 – Part 1: Downward transport of upper atmospheric NO<sub>x</sub> produced by low energy electrons, *Atmos. Chem. Phys.*, 9, 2729–2740, doi:10.5194/acp-9-2729-2009, 2009. 30173, 30175, 30176, 30182
- 15 Baumgaertner, A. J. G., Jöckel, P., Riede, H., Stiller, G., and Funke, B.: Energetic particle precipitation in ECHAM5/MESSy – Part 2: Solar proton events, *Atmos. Chem. Phys.*, 10, 7285–7302, doi:10.5194/acp-10-7285-2010, 2010. 30176
- Boberg, F. and Lundstedt, H.: Solar Wind Variations Related to Fluctuations of the North Atlantic Oscillation, *Geophys. Res. Lett.*, 29, 1718, doi:10.1029/2002GL014903, 2002. 30173
- Brühl, C., Steil, B., Stiller, G., Funke, B., and Jöckel, P.: Nitrogen compounds and ozone in the stratosphere: comparison of MIPAS satellite data with the chemistry climate model ECHAM5/MESSy1, *Atmos. Chem. Phys.*, 7, 5585–5598, doi:10.5194/acp-7-5585-2007, 2007. 30175
- 25 Christiansen, B., Guldberg, A., Hansen, A. W., and Riishøjgaard, L. P.: On the response of a three-dimensional general circulation model to imposed changes in the ozone distribution, *J. Geophys. Res.*, 102, 13051–13078, doi:10.1029/97JD00529, 1997. 30182
- 30 Clilverd, M. A., Rodger, C. J., and Ulich, T.: The importance of atmospheric precipitation in storm-time relativistic electron flux drop outs, *Geophys. Res. Lett.*, 33, L01102, doi:10.1029/2005GL024661, 2006. 30173

### High altitude NO<sub>x</sub> modulation of the NAM index

A. J. G. Baumgaertner  
et al.

Title Page

Abstract

Introduction

Conclusions

References

Tables

Figures

◀

▶

◀

▶

Back

Close

Full Screen / Esc

Printer-friendly Version

Interactive Discussion



---

**High altitude NO<sub>x</sub>  
modulation of the  
NAM index**A. J. G. Baumgaertner  
et al.

---

Title Page

Abstract

Introduction

Conclusions

References

Tables

Figures

◀

▶

◀

▶

Back

Close

Full Screen / Esc

Printer-friendly Version

Interactive Discussion



Funke, B., López-Puertas, M., Gil-López, S., von Clarmann, T., Stiller, G. P., Fischer, H., and Kellmann, S.: Downward transport of upper atmospheric NO<sub>x</sub> into the polar stratosphere and lower mesosphere during the Antarctic 2003 and Arctic 2002/2003 winters, *J. Geophys. Res.*, 110, D24308, doi:10.1029/2005JD006463, 2005. 30173, 30175

5 Gruzdev, A. N., Schmidt, H., and Brasseur, G. P.: The effect of the solar rotational irradiance variation on the middle and upper atmosphere calculated by a three-dimensional chemistry-climate model, *Atmos. Chem. Phys.*, 9, 595–614, doi:10.5194/acp-9-595-2009, 2009. 30173

Hood, L. L. and Soukharev, B. E.: Solar induced variations of odd nitrogen: Multiple regression analysis of UARS HALOE data, *Geophys. Res. Lett.*, 33, L22805, doi:10.1029/2006GL028122, doi:10.1029/2006GL028122, 2006. 30173

10 Hurrell, J. and Kushnir, Y. (Eds.): *The North Atlantic Oscillation: Climate Significance and Environmental Impact*, vol. 134 of Geophysical Monograph Series, AGU, 2003. 30184

IPCC: *IPCC Fourth Assessment Report: Climate Change 2007*, Cambridge University Press, Cambridge, 2007. 30173

15 Jöckel, P., Tost, H., Pozzer, A., Brühl, C., Buchholz, J., Ganzeveld, L., Hoor, P., Kerkweg, A., Lawrence, M. G., Sander, R., Steil, B., Stiller, G., Tanarhte, M., Taraborrelli, D., van Aardenne, J., and Lelieveld, J.: The atmospheric chemistry general circulation model ECHAM5/MESy1: consistent simulation of ozone from the surface to the mesosphere, *Atmos. Chem. Phys.*, 6, 5067–5104, doi:10.5194/acp-6-5067-2006, 2006. 30174, 30175

20 Jöckel, P., Kerkweg, A., Pozzer, A., Sander, R., Tost, H., Riede, H., Baumgaertner, A., Gromov, S., and Kern, B.: Development cycle 2 of the Modular Earth Submodel System (MESy2), *Geosci. Model Dev. Discuss.*, 3, 1423–1501, doi:10.5194/gmdd-3-1423-2010, 2010. 30174

Langematz, U., Kunze, M., Krüger, K., Labitzke, K., and Roff, G. L.: Thermal and dynamical changes of the stratosphere since 1979 and their link to ozone and CO<sub>2</sub> changes, *J. Geophys. Res.*, 108, 4027, doi:10.1029/2002JD002069, 2003. 30182, 30183

25 Lelieveld, J., Brühl, C., Jöckel, P., Steil, B., Crutzen, P. J., Fischer, H., Giorgetta, M. A., Hoor, P., Lawrence, M. G., Sausen, R., and Tost, H.: Stratospheric dryness: model simulations and satellite observations, *Atmos. Chem. Phys.*, 7, 1313–1332, doi:10.5194/acp-7-1313-2007, 2007. 30175

30 Lu, H., Clilverd, M. A., Seppälä, A., and Hood, L. L.: Geomagnetic perturbations on stratospheric circulation in late winter and spring, *J. Geophys. Res.*, 113, D16106, doi:10.1029/2007JD008915, 2008. 30174

Mayaud, P. N.: *Derivation, Meaning, and Use of Geomagnetic Indices*, Geophysical Monograph

## High altitude NO<sub>x</sub> modulation of the NAM index

A. J. G. Baumgaertner  
et al.

Title Page

Abstract

Introduction

Conclusions

References

Tables

Figures

◀

▶

◀

▶

Back

Close

Full Screen / Esc

Printer-friendly Version

Interactive Discussion

22, Am. Geophys. Union, Washington D.C., 1980. 30174

Meehl, G. A., Arblaster, J. M., Matthes, K., Sassi, F., and van Loon, H.: Amplifying the Pacific climate system response to a small 11 year solar cycle forcing, *Science*, 325, 1114–1118, 2009. 30173

5 Nissen, K. M., Matthes, K., Langematz, U., and Mayer, B.: Towards a better representation of the solar cycle in general circulation models, *Atmos. Chem. Phys.*, 7, 5391–5400, doi:10.5194/acp-7-5391-2007, 2007. 30175, 30176

Randall, C. E., Harvey, V. L., Manney, G. L., Orsolini, Y., Codrescu, M., Sioris, C., Brohede, S., Haley, C. S., Gordley, L. L., Zawodny, J. M., and Russell, J. M.: Stratospheric effects of energetic particle precipitation in 2003-2004, *Geophys. Res. Lett.*, 32, L05802, doi:10.1029/2004GL022003, 2005. 30173, 30175

Randall, C. E., Harvey, V. L., Singleton, C. S., Bailey, S. M., Bernath, P. F., Codrescu, M., Nakajima, H., and Russell, J. M.: Energetic particle precipitation effects on the Southern Hemisphere stratosphere in 1992-2005, *J. Geophys. Res.*, 112, D08308, doi:10.1029/2006JD007696, 2007. 30173

Randel, W. J. and Wu, F.: Cooling of the Arctic and Antarctic polar stratospheres due to ozone depletion., *J. Climate*, 12, 1467–1479, doi:10.1175/1520-0442(1999)012<1467:COTAAA>2.0.CO;2, 1999. 30182

Rayner, N. A., Parker, D. E., Horton, E. B., Folland, C. K., Alexander, L. V., Rowell, D. P., Kent, E. C., and Kaplan, A.: Global analyses of sea surface temperature, sea ice, and night marine air temperature since the late nineteenth century, *J. Geophys. Res.*, 108(D14), 4407, doi:10.1029/2002JD002670, 2003. 30177

20 Roeckner, E., Brokopf, R., Esch, M., Giorgetta, M., Hagemann, S., Kornblueh, L., Manzini, E., Schlese, U., and Schulzweida, U.: Sensitivity of simulated climate to horizontal and vertical resolution in the ECHAM5 atmosphere model, *J. Climate*, 19, 3771, doi:10.1175/JCLI3824.1, 2006. 30175

25 Rozanov, E., Callis, L., Schlesinger, M., Yang, F., Andronova, N., and Zubov, V.: Atmospheric response to NO<sub>y</sub> source due to energetic electron precipitation, *Geophys. Res. Lett.*, 32, L14811, doi:10.1029/2005GL023041, 2005. 30174

30 Sander, R., Kerkweg, A., Jöckel, P., and Lelieveld, J.: Technical note: The new comprehensive atmospheric chemistry module MECCA, *Atmos. Chem. Phys.*, 5, 445–450, doi:10.5194/acp-5-445-2005, 2005. 30175

Seppälä, A., Clilverd, M. A., and Rodger, C. J.: NO<sub>x</sub> enhancements in the middle atmosphere

**High altitude NO<sub>x</sub>  
modulation of the  
NAM index**A. J. G. Baumgaertner  
et al.

Title Page

Abstract

Introduction

Conclusions

References

Tables

Figures

◀

▶

◀

▶

Back

Close

Full Screen / Esc

Printer-friendly Version

Interactive Discussion



during 2003-2004 polar winter: Relative significance of solar proton events and the aurora as a source, *J. Geophys. Res.*, 112, D23303, doi:10.1029/2006JD008326, 2007a. 30173

Seppälä, A., Verronen, P. T., Ciliverd, M. A., Randall, C. E., Tamminen, J., Sofieva, V., Backman, L., and Kyrölä, E.: Arctic and Antarctic polar winter NO<sub>x</sub> and energetic particle precipitation in 2002-2006, *Geophys. Res. Lett.*, 34, L12810, doi:10.1029/2007GL029733, 2007b. 30173, 30180

Seppälä, A., Randall, C. E., Ciliverd, M. A., Rozanov, E., and Rodger, C. J.: Geomagnetic activity and polar surface air temperature variability, *J. Geophys. Res.*, 114, A10312, doi:10.1029/2008JA014029, 2009. 30174, 30176, 30177, 30179, 30180, 30181, 30184, 30191

Shine, K. P., Bourqui, M. S., Forster, P. M. D. F., Hare, S. H. E., Langematz, U., Braesicke, P., Grewe, V., Ponater, M., Schnadt, C., Smith, C. A., Haigh, J. D., Austin, J., Butchart, N., Shindell, D. T., Randel, W. J., Nagashima, T., Portmann, R. W., Solomon, S., Seidel, D. J., Lanzante, J., Klein, S., Ramaswamy, V., and Schwarzkopf, M. D.: A comparison of model-simulated trends in stratospheric temperatures, *Q. J. Roy. Meteorol. Soc.*, 129, 1565–1588, doi:10.1256/qj.02.186, 2003. 30182

Siskind, D. E., Nedoluha, G. E., Randall, C. E., Fromm, M., and Russell III, J. M.: An assessment of Southern Hemisphere stratospheric NO<sub>x</sub> enhancements due to transport from the upper atmosphere, *Geophys. Res. Lett.*, 27, 329–332, doi:10.1029/1999GL010940, 2000. 30173

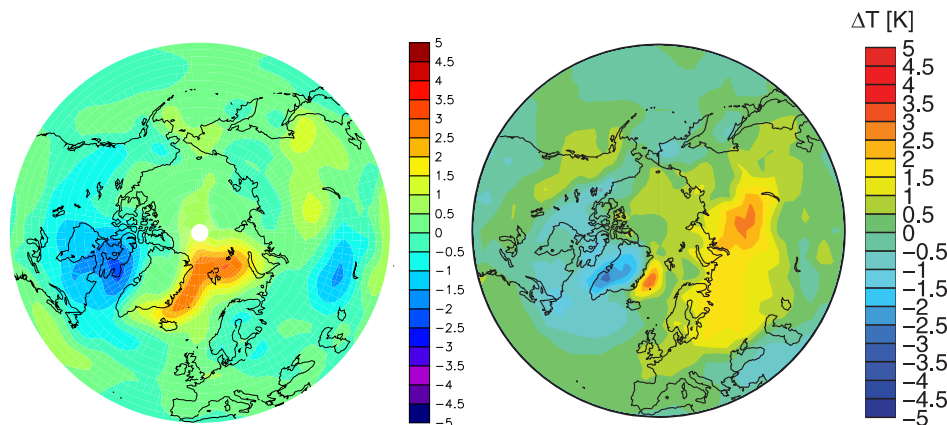
Thejll, P., Christiansen, B., and Gleisner, H.: On correlations between the North Atlantic Oscillation, geopotential heights, and geomagnetic activity, *Geophys. Res. Lett.*, 30, 1347, doi:10.1029/2002GL016598, 2003. 30173

Uppala, S. M., Kållberg, P. W., Simmons, A. J., Andrae, U., Bechtold, V. D. C., Fiorino, M., Gibson, J. K., Haseler, J., Hernandez, A., Kelly, G. A., Li, X., Onogi, K., Saarinen, S., Sokka, N., Allan, R. P., Andersson, E., Arpe, K., Balmaseda, M. A., Beljaars, A. C. M., Berg, L. V. D., Bidlot, J., Bormann, N., Caires, S., Chevallier, F., Dethof, A., Dragosavac, M., Fisher, M., Fuentes, M., Hagemann, S., Hólm, E., Hoskins, B. J., Isaksen, I., Janssen, P. A. E. M., Jenne, R., McNally, A. P., Mahfouf, J., Morcrette, J., Rayner, N. A., Saunders, R. W., Simon, P., Sterl, A., Trenberth, K. E., Untch, A., Vasiljevic, D., Viterbo, P., and Woollen, J.: The ERA-40 re-analysis, *Q. J. Roy. Meteorol. Soc.*, 131, 2961–3012, doi:10.1256/qj.04.176, 2005. 30174



## High altitude $\text{NO}_x$ modulation of the NAM index

A. J. G. Baumgaertner  
et al.

[Title Page](#)[Abstract](#)[Introduction](#)[Conclusions](#)[References](#)[Tables](#)[Figures](#)[◀](#)[▶](#)[◀](#)[▶](#)[Back](#)[Close](#)[Full Screen / Esc](#)[Printer-friendly Version](#)[Interactive Discussion](#)

**Fig. 1.** Left: Northern Hemisphere DJF surface temperature difference between years of high and low geomagnetic activity (see Table 1). Left: transient simulation (S-TRANSIENT), right: from ERA-40 reanalysis data, taken from (Seppälä et al., 2009, their Fig. 2). Red/blue colours indicate positive/negative differences.

## High altitude $\text{NO}_x$ modulation of the NAM index

A. J. G. Baumgaertner  
et al.

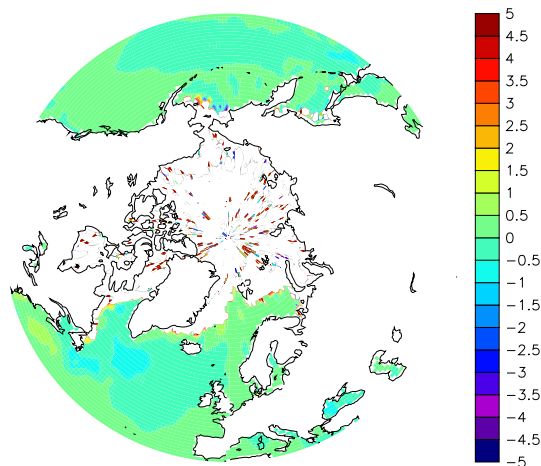


**Fig. 2.** As Fig. 1 (left) but for sea surface temperatures from HadISST1 dataset as used in the simulation S-TRANSIENT.

[Title Page](#)[Abstract](#)[Introduction](#)[Conclusions](#)[References](#)[Tables](#)[Figures](#)[◀](#)[▶](#)[◀](#)[▶](#)[Back](#)[Close](#)[Full Screen / Esc](#)[Printer-friendly Version](#)[Interactive Discussion](#)

## High altitude $\text{NO}_x$ modulation of the NAM index

A. J. G. Baumgaertner  
et al.

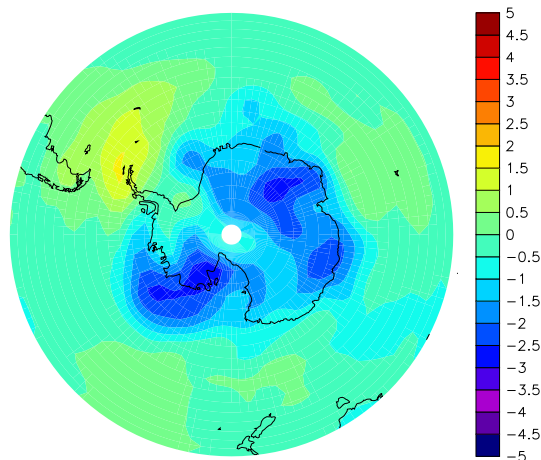
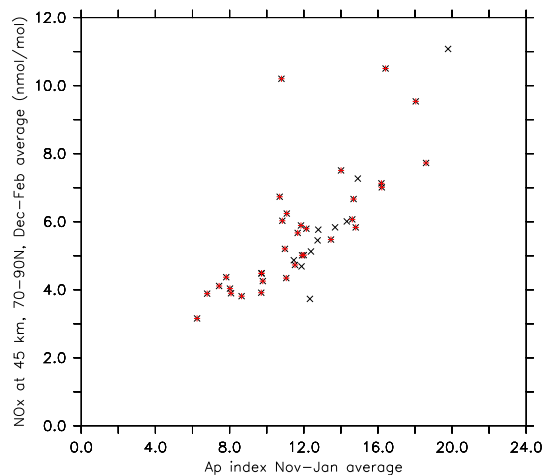


**Fig. 3.** Southern Hemisphere JJA temperature difference between years of high and low geomagnetic activity (see Table 1) from the transient simulation.

[Title Page](#)[Abstract](#)[Introduction](#)[Conclusions](#)[References](#)[Tables](#)[Figures](#)[◀](#)[▶](#)[◀](#)[▶](#)[Back](#)[Close](#)[Full Screen / Esc](#)[Printer-friendly Version](#)[Interactive Discussion](#)

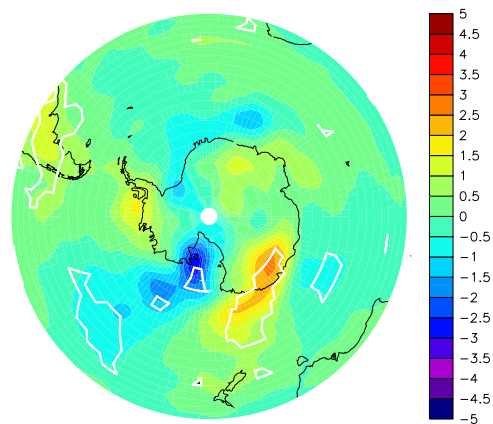
## High altitude $\text{NO}_x$ modulation of the NAM index

A. J. G. Baumgaertner  
et al.



**Fig. 4.** Ap index versus  $\text{NO}_x$  mixing ratios (nmol/mol) at 45 km altitude for Northern Hemisphere winters, from the transient simulation. Black crosses: all available years, red stars: selected years according to Table 1.

[Title Page](#)[Abstract](#)[Introduction](#)[Conclusions](#)[References](#)[Tables](#)[Figures](#)[◀](#)[▶](#)[◀](#)[▶](#)[Back](#)[Close](#)[Full Screen / Esc](#)[Printer-friendly Version](#)[Interactive Discussion](#)

**High altitude NO<sub>x</sub>  
modulation of the  
NAM index**A. J. G. Baumgaertner  
et al.

**Fig. 5.** Southern Hemisphere JJA surface temperature difference (K),  $\Delta T = T^{\text{S-EPP}} - T^{\text{S-noEPP}}$ .

Title Page

Abstract

Introduction

Conclusions

References

Tables

Figures

◀

▶

◀

▶

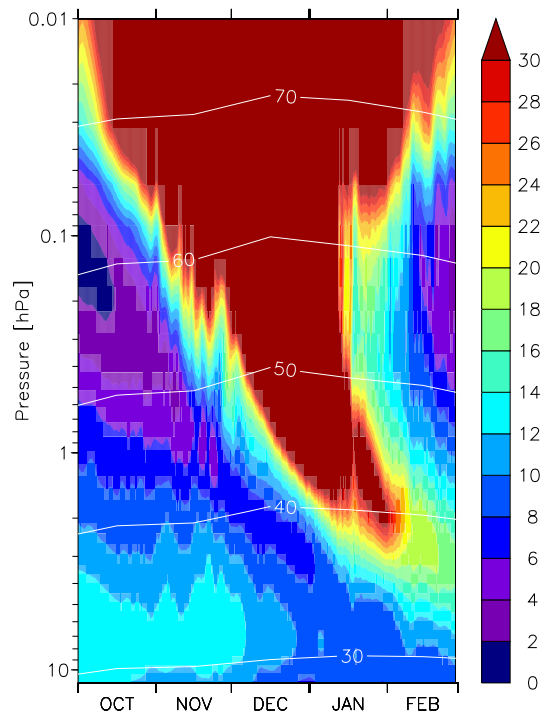
Back

Close

Full Screen / Esc

Printer-friendly Version

Interactive Discussion

**High altitude NO<sub>x</sub> modulation of the NAM index**A. J. G. Baumgaertner  
et al.

**Fig. 6.** Zonal mean NO<sub>x</sub> mixing ratios (nmol/mol) from simulation S-EPP for a Northern Hemisphere winter poleward of 60° N. The white contour lines denote the altitude in km.

[Title Page](#)[Abstract](#)[Introduction](#)[Conclusions](#)[References](#)[Tables](#)[Figures](#)[◀](#)[▶](#)[◀](#)[▶](#)[Back](#)[Close](#)[Full Screen / Esc](#)[Printer-friendly Version](#)[Interactive Discussion](#)

## High altitude NO<sub>x</sub> modulation of the NAM index

A. J. G. Baumgaertner  
et al.

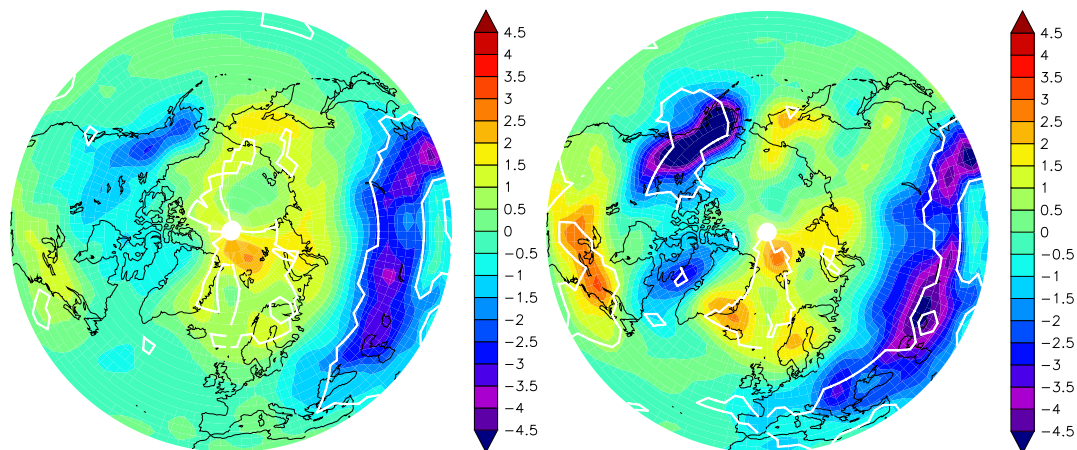


**Fig. 7.** NH DJF surface temperature difference  $\Delta T = T^{\text{S-EPP}} - T^{\text{S-noEPP}}$ . Left: all years, right: only years without SSWs.

[Title Page](#)[Abstract](#)[Introduction](#)[Conclusions](#)[References](#)[Tables](#)[Figures](#)[◀](#)[▶](#)[◀](#)[▶](#)[Back](#)[Close](#)[Full Screen / Esc](#)[Printer-friendly Version](#)[Interactive Discussion](#)

## High altitude $\text{NO}_x$ modulation of the NAM index

A. J. G. Baumgaertner  
et al.

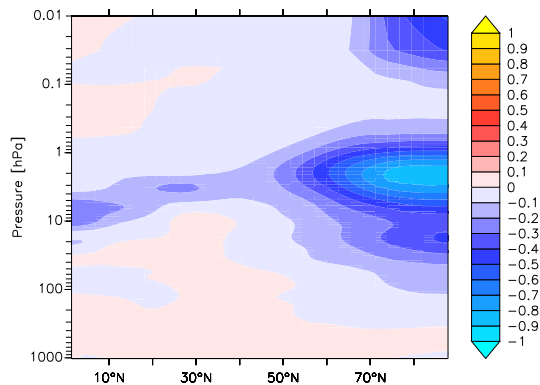


**Fig. 8.** Climatological DJF change ( $\mu\text{mol mol}^{-1}$ ) of ozone,  $\Delta\text{O}_3 = \text{O}_3^{\text{S-EPP}} - \text{O}_3^{\text{S-noEPP}}$ . Red-yellow/blue colours indicate positive/negative differences.

[Title Page](#)[Abstract](#)[Introduction](#)[Conclusions](#)[References](#)[Tables](#)[Figures](#)[◀](#)[▶](#)[◀](#)[▶](#)[Back](#)[Close](#)[Full Screen / Esc](#)[Printer-friendly Version](#)[Interactive Discussion](#)

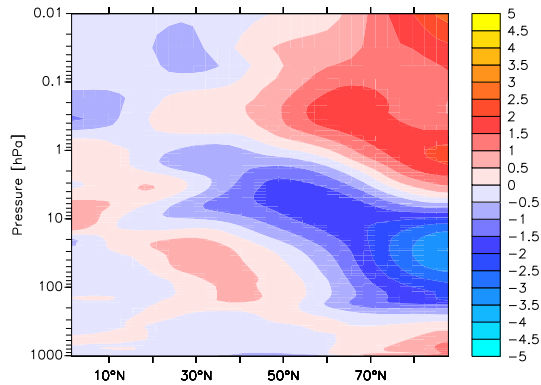


**Fig. 9.** Climatological DJF change of temperature (K),  $\Delta T = T^{\text{S-EPP}} - T^{\text{S-noEPP}}$ .

**High altitude NO<sub>x</sub> modulation of the NAM index**

A. J. G. Baumgaertner et al.

Title Page

Abstract Introduction

Conclusions References

Tables Figures

◀ ▶

◀ ▶

Back Close

Full Screen / Esc

Printer-friendly Version

Interactive Discussion



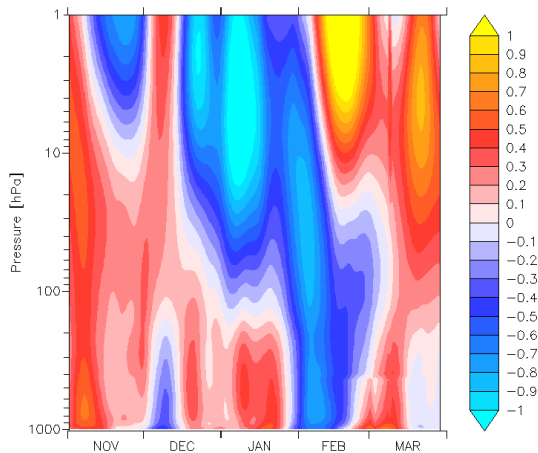


**Fig. 10.** Climatological change of geopotential height anomalies (normalised) for the region 60° N–90° N,  $\Delta Z = Z^{\text{S-EPP}} - Z^{\text{S-noEPP}}$ .

**High altitude NO<sub>x</sub> modulation of the NAM index**

A. J. G. Baumgaertner et al.

Title Page

Abstract Introduction

Conclusions References

Tables Figures

◀ ▶

◀ ▶

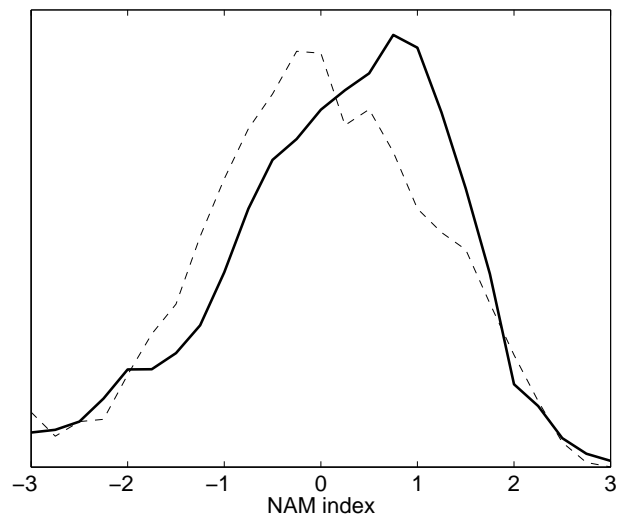
Back Close

Full Screen / Esc

Printer-friendly Version

Interactive Discussion



**High altitude NO<sub>x</sub>  
modulation of the  
NAM index**A. J. G. Baumgaertner  
et al.

**Fig. 11.** NAM index histogram for the altitude region 10 hPa–200 hPa for DJF. Solid: S-EPP, dotted: S-noEPP.

[Title Page](#)[Abstract](#)[Introduction](#)[Conclusions](#)[References](#)[Tables](#)[Figures](#)[◀](#)[▶](#)[◀](#)[▶](#)[Back](#)[Close](#)[Full Screen / Esc](#)[Printer-friendly Version](#)[Interactive Discussion](#)

**High altitude NO<sub>x</sub> modulation of the NAM index**

A. J. G. Baumgaertner et al.

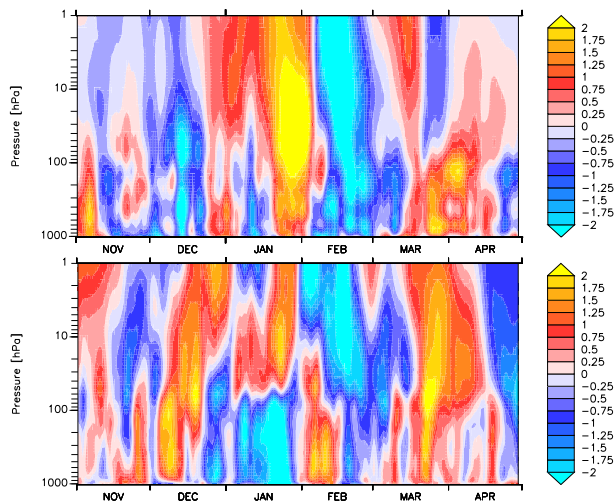


**Fig. 12.** NAM index for a single winter calculated from simulation S-EPP (top) and S-noEPP (bottom).

Title Page

Abstract Introduction

Conclusions References

Tables Figures

◀ ▶

◀ ▶

Back Close

Full Screen / Esc

Printer-friendly Version

Interactive Discussion



## High altitude NO<sub>x</sub> modulation of the NAM index

A. J. G. Baumgaertner  
et al.

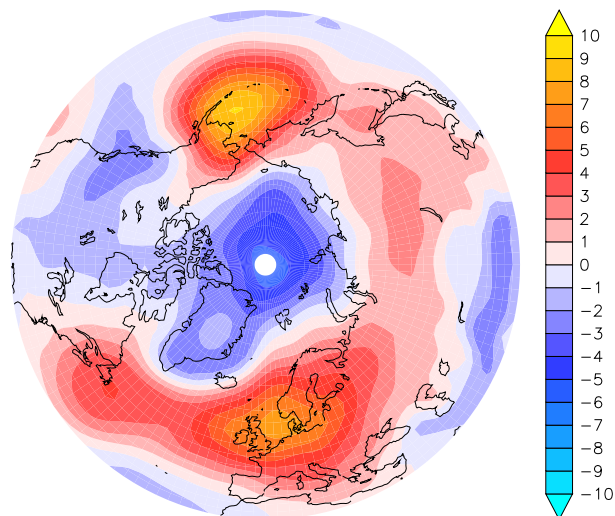


**Fig. 13.** DJF surface pressure difference (hPa)  $\Delta p = p^{\text{S-EPP}} - p^{\text{S-noEPP}}$ , SSW years excluded.

Title Page

Abstract

Introduction

Conclusions

References

Tables

Figures

◀

▶

◀

▶

Back

Close

Full Screen / Esc

Printer-friendly Version

Interactive Discussion